Approach to approximating the pair distribution function of inhomogeneous hard-sphere fluids

Paho Lurie-Gregg, Jeff B. Schulte, and David Roundy
Department of Physics, Oregon State University, Corvallis, Oregon 97331, USA
(Received 26 March 2014; revised manuscript received 17 July 2014; published 21 October 2014)

We introduce an approximation for the pair distribution function of the inhomogeneous hard sphere fluid. Our approximation makes use of our recently published averaged pair distribution function at contact, which has been shown to accurately reproduce the averaged pair distribution function at contact for inhomogeneous density distributions. This approach achieves greater computational efficiency than previous approaches by enabling the use of exclusively fixed-kernel convolutions and thus allowing an implementation using fast Fourier transforms. We compare results for our pair distribution approximation with two previously published works and Monte Carlo simulation, showing favorable results.

DOI: 10.1103/PhysRevE.90.042130 PACS number(s): 61.20.Ne

I. INTRODUCTION

The standard approach in liquid state theory is to model a liquid as a hard-sphere reference fluid with attractive interactions that are treated perturbatively [1]. Recent advances have extended these perturbative approaches to inhomogeneous density distributions, that is, liquid interfaces, through the use of classical density functional theory (DFT), in which the grand free energy is found by minimizing a free-energy functional of the density [2–10]. The perturbation theory treatment of intermolecular interactions relies on the pair distribution function of the reference fluid: $g^{(2)}_{HS}(\mathbf{r}_1,\mathbf{r}_2)$. Unlike the radial distribution function of a homogeneous fluid, there does not currently exist a tractable form for the pair distribution function of an inhomogeneous hard-sphere fluid suitable for use in constructing a density functional [2,3].

At its core, thermodynamic perturbation theory (TPT), sometimes referred to as the high-temperature expansion, is an expansion of the free energy in powers of a small parameter, which is the product of a pairwise attractive interaction with the inverse temperature β:

$$F = F_0 + F_1 + \beta F_2 + O(\beta^2), \tag{1}$$

where the terms F_n are corrections to the free energy of order n in the small interaction. The first and largest term in this expansion is

$$F_1[n(\mathbf{r})] = \frac{1}{2}\iint g^{(2)}_{HS}(\mathbf{r}_1,\mathbf{r}_2)n(\mathbf{r}_1)n(\mathbf{r}_2)\Phi(|\mathbf{r}_1-\mathbf{r}_2|)d\mathbf{r}_1\,d\mathbf{r}_2, \tag{2}$$

where $g^{(2)}_{HS}(\mathbf{r}_1,\mathbf{r}_2)$ is the pair distribution function of the hard-sphere reference fluid, and $\Phi(r)$ is the pair potential. Formally, this requires the pair distribution function as a functional of the density $n(\mathbf{r})$. In Sec. II we introduce existing theoretical approaches for computing $g^{(2)}_{HS}(\mathbf{r}_1,\mathbf{r}_2)$ given the external potential felt by the hard spheres. In Sec. III we introduce existing approximations for the hard-sphere pair distribution that are expressed as a functional of the density distribution $n(\mathbf{r})$, which is a form that is more directly useful in the construction of classical density functionals, which are themselves expressed as a functional of the density.

In this paper, we introduce a new contact value approach (CVA) to approximating the hard-sphere pair distribution function which is suitable for use in the creation of classical density functionals based on thermodynamic perturbation theory. The resulting function is based on a fit to the radial distribution function that is separable in a way that enables efficient evaluation of the integral in Eq. (2).

II. PAIR DISTRIBUTION FROM THE EXTERNAL POTENTIAL

Given the external potential $V(\mathbf{r})$ felt by a hard-sphere fluid, several approaches have been used to compute the pair distribution function. We review these approaches here. The classic (and earliest) approach for computing the pair distribution function given the external potential is Percus's trick of treating one sphere as an additional contribution to the external potential and to find the pair distribution function from the resultant equilibrium density [1]. This elegant approach lends itself to computation *using* DFT, and can be used to compute and plot the pair distribution function, but requires a full free-energy minimization *for each position* $\mathbf{r}_1$ in $g^{(2)}(\mathbf{r}_1,\mathbf{r}_2)$ and hence would be prohibitively expensive as a tool in constructing a free-energy functional.

The canonical inhomogeneous configuration for the hard-sphere fluid is the system consisting of a hard sphere at a hard wall. In 1986 Plischke and Henderson solved the pair distribution function of this system using integral equation theory under the Percus-Yevick approximation [11]. Lado recently introduced a new and more efficient algorithm for implementing integral equation theory for inhomogeneous fluids, which computes $g^{(2)}(\mathbf{r}_1,\mathbf{r}_2)$ [12]. While this approach is two orders of magnitude more efficient than previous implementations, it remains a computationally expensive approach and unsuitable for repeated evaluation within a free-energy minimization as required by DFT.

Another inhomogeneous configuration that is of interest is the test-particle configuration, in which one hard sphere is fixed. Where the hard-wall is a surface with no curvature, the test-particle configuration has a surface with curvature at the molecular length scale. In this case, the density gives the radial distribution function (this is just Percus's trick), and the pair distribution function of this inhomogeneous test-particle system gives the triplet distribution function of the homogeneous fluid. The triplet distribution function of the homogeneous fluid has been computed by González *et al.* using the test-particle approach with *two* spheres fixed [13].

III. PAIR DISTRIBUTION FROM THE DENSITY

The alternative to specifying the external potential is to specify the density distribution $n(\mathbf{r})$. One may move between these representations by either computing the external potential corresponding to a given density of hard spheres by taking a functional derivative of the hard-sphere free-energy functional or by minimizing the free energy given an external potential. However, in general it is simplest to use an approach that makes use of the natural variables, which in the case of classical density functional theory is the density.

The most direct and rigorous approach to find the pair distribution function given the density is to take a second functional derivative of the hard-sphere free energy to find the direct correlation function. One can then solve the Ornstein-Zernike equation numerically to find the pair distribution function. This approach was used by Götzelmann *et al.* to solve for the pair distribution function near a hard wall using an early hard-sphere free-energy functional [14]. While this approach is rigorous, solving the inhomogeneous Ornstein-Zernike equation remains computationally challenging, although more efficient approximate algorithms have been developed [15]. This approach, while appealing, remains unsuitable for use in the construction of a classical density functional due to its significant computational cost.

In addition to the above exact approach, there are a number of analytic approximations for the inhomogeneous pair distribution function, which extend the radial distribution function to inhomogeneous scenarios. These approximations differ both in what density to use when evaluating the radial distribution function $g(r;n)$ and in how to combine the radial distribution function evaluated at these densities [16].

Early approximations to the pair distribution function used the density at one or two positions to determine the pair distribution function. There are three common approaches:

$$g^{(2)}(\mathbf{r}_1,\mathbf{r}_2) \approx g\left(r_{12}; n\left(\frac{\mathbf{r}_1+\mathbf{r}_2}{2}\right)\right) \text{midpoint}, \tag{3}$$

$$g^{(2)}(\mathbf{r}_1,\mathbf{r}_2) \approx g\left(r_{12}; \frac{n(\mathbf{r}_1)+n(\mathbf{r}_2)}{2}\right) \text{mean density}, \tag{4}$$

$$g^{(2)}(\mathbf{r}_1,\mathbf{r}_2) \approx \frac{g(r_{12};n(\mathbf{r}_1))+g(r_{12};n(\mathbf{r}_2))}{2} \text{mean function}. \tag{5}$$

These approaches have been successfully and widely used in treating the surface tension of simple fluids [17–25]. The mean density approximation has also been quoted (as a goal) by recent papers that proceed to make further approximations [3,4]. However, these approximations fail dramatically when applied to strongly inhomogeneous systems such as a dense fluid at a solid surface. Such systems exhibit a strongly oscillatory density distribution, with density peaks that can have local packing fractions greater than unity, which cannot occur in the bulk reference system that defines $g(r;n)$. The above papers restrict themselves to the liquid-vapor interface, which does not exhibit this pathology.

Nonpathological approaches use an average of the density over some volume. Fischer and Methfessel introduce the approximation [26,27]

$$g^{(2)}(\mathbf{r}_1,\mathbf{r}_2) \approx g\left(r_{12}; n_3\left(\tfrac{1}{2}[\mathbf{r}_1+\mathbf{r}_2)\right)\right), \tag{6}$$

where n_3 is an integral of the density over a spherical volume that is now used as one of the fundamental measures in Fundamental Measure Theory (FMT) [28]:

$$n_3(\mathbf{r}) = \int n(\mathbf{r}')\Theta\left(\tfrac{1}{2}\sigma - |\mathbf{r}-\mathbf{r}'|\right) d\mathbf{r}'. \tag{7}$$

Equation (6) is computationally awkward because it treats as special the midpoint $\frac{1}{2}(\mathbf{r}_1+\mathbf{r}_2)$. Moreover, the approach of Fischer and Methfessel is intended to approximate the pair distribution function only at contact, when the distance between $\mathbf{r}_1$ and $\mathbf{r}_2$ is the hard-sphere diameter. Tang *et al.* employed an approximation for the pair distribution function that is similar to that of Fischer and Methfessel, but with a self-consistent weighted density computed with a weighting function that is itself dependent on the weighted density [29]. This weighted density was computed using the hard-sphere weighted density of Tarazona, which was developed using the direct correlation function of the homogeneous hard-sphere fluid [30].

Sokolowski and Fischer addressed the shortcomings of the theory of Fischer and Methfessel by modifying this approach to use density averages centered on the two points $\mathbf{r}_1$ and $\mathbf{r}_2$:

$$g^{(2)}(\mathbf{r}_1,\mathbf{r}_2) \approx g\left(r_{12}; \tfrac{1}{2}[\bar{n}(\mathbf{r}_1)+\bar{n}(\mathbf{r}_2)]\right), \tag{8}$$

where their averaged density $\bar{n}(\mathbf{r})$ given by

$$\bar{n}(\mathbf{r}) \equiv \frac{3}{4\pi(0.8\sigma)^3}\int n(\mathbf{r}')\Theta(0.8\sigma - |\mathbf{r}-\mathbf{r}'|)\, d\mathbf{r}' \tag{9}$$

is the density averaged over a sphere with diameter 0.8σ [31]. The value 0.8 in this formula was arrived at by fitting to Monte Carlo simulation. Although Eq. (8) has the advantage of only involving density averages at the points at which the pair distribution function is desired, it remains sufficiently computationally cumbersome that it has been used in only two papers studying the one-dimensional liquid vapor interface [32,33]. Because it cannot be written as a single-site convolution, this approach is particularly computationally demanding when applied to systems featuring inhomogeneity in more than one dimension.

In a previous paper [34], we introduced a functional that gives a good approximation for the pair distribution function averaged over positions $\mathbf{r}_2$ that are in contact with $\mathbf{r}_1$, defined as

$$g_\sigma(\mathbf{r}_1) \equiv \frac{\int g^{(2)}(\mathbf{r}_1,\mathbf{r}_2)\delta(\sigma - |\mathbf{r}_1-\mathbf{r}_2|)n(\mathbf{r}_2)\, d\mathbf{r}_2}{\tilde{n}(\mathbf{r}_1)}, \tag{10}$$

where the weighted density $\tilde{n}(\mathbf{r}_1)$ is defined by

$$\tilde{n}(\mathbf{r}) \equiv \int n(\mathbf{r}')\delta(\sigma - |\mathbf{r}-\mathbf{r}'|)\, d\mathbf{r}'. \tag{11}$$

In Ref. [34] we use the contact-value theorem to derive the exact formula:

$$g_\sigma(\mathbf{r}) = \frac{1}{2}\frac{1}{k_B T n(\mathbf{r})\tilde{n}(\mathbf{r})}\frac{\delta F_{HS}}{\delta\sigma(\mathbf{r})}, \tag{12}$$

where $\sigma(\mathbf{r})$ is the diameter of hard spheres located at position $\mathbf{r}$, and F_{HS} is the Helmholtz free energy of the hard-sphere fluid. The functional derivative of the free energy with respect to the hard-sphere diameter in Eq. (12) requires that we be able to evaluate the change in free energy resulting from a change in the diameter of specifically the hard spheres located at position $\mathbf{r}$. This somewhat unusual construction is mathematically straightforward within FMT [28]. We employ the White Bear variation of the FMT free-energy functional [35], which provides an excellent approximation for this averaged value of the pair distribution function at contact for a variety of interfaces and over a wide range of densities.

IV. CONTACT VALUE APPROACH

In the approaches for the pair distribution function mentioned above, the radial distribution function used in the approximation was dependent upon the density averaged over some volume. We seek to achieve greater accuracy by making use of a function dependent upon our averaged $g_\sigma(\mathbf{r})$ discussed above, which holds more information about an inhomogeneous system than does a simple convolution of the density. We construct the CVA with the average of two radial distribution functions, evaluated at the distance between the two points, that are themselves functions of the averaged pair distribution function at contact $g_\sigma(\mathbf{r})$ evaluated at the two points:

$$g^{(2)}(\mathbf{r}_1,\mathbf{r}_2) = \frac{g(r_{12}; g_\sigma(\mathbf{r}_1)) + g(r_{12}; g_\sigma(\mathbf{r}_2))}{2}. \quad (13)$$

This CVA for $g^{(2)}(\mathbf{r}_1,\mathbf{r}_2)$ is constructed to reproduce the exact value for the integral:

$$F_1^{\text{contact}} = \frac{1}{2}\iint g_{HS}^{(2)}(\mathbf{r}_1,\mathbf{r}_2) n(\mathbf{r}_1) n(\mathbf{r}_2) \delta(|\mathbf{r}_1 - \mathbf{r}_2| - \sigma) \times d\mathbf{r}_1\, d\mathbf{r}_2, \quad (14)$$

which is the mean-field correction to the free energy [see Eq. (2)] for a purely contact interaction.

The CVA requires the radial distribution function expressed as a function of r and g_σ. We construct a functional form for $g(r, g_\sigma)$ that allows for improved computational efficiency. We introduce the general form that allows for this efficiency in Sec. V, and we detail our specific approximation for $g(r, g_\sigma)$ that uses this general form in Sec. VI.

V. MAKING THE CVA EFFICIENT

The existing approaches to approximating the pair distribution function outlined in Sec. III have not been widely used in the construction of density functionals based on thermodynamic perturbation theory, largely due to their computational complexity. While our CVA provides only an incremental improvement in accuracy, its construction enables significant gains in computational efficiency, allowing for practical application in density functionals. We achieve this gain by developing a *separable* fit to the radial distribution function of the hard-sphere fluid (see Sec. VI for details). This separable fit is of the form

$$g(r; g_\sigma) = \sum_i a_i(r) b_i(g_\sigma), \quad (15)$$

where the notable aspect is that the radial distribution function is written as a sum of terms that are each a simple product of a function of radius with a function of g_σ. This enables us to write integrals, such as Eq. (2), that are linear in the pair distribution function as a summation of fixed-kernel convolutions, which may be efficiently computed using fast Fourier transforms (FFTs).

Computation of the free-energy correction from Eq. (2) for a periodic system by direct integration requires a nested integration over the volume of the system V_{cell} and the volume over which the interaction is nonzero V_Φ. Thus the cost of computation scales as $O(\frac{V_{cell}V_\Phi}{\Delta V^2})$ where ΔV is the volume resolution of the computational grid. Direct integration is the most efficient algorithm when using the existing functionals for $g^{(2)}(\mathbf{r}_1,\mathbf{r}_2)$ described in Sec. III. The one exception is the "mean-function" approximation [Eq. (5)], which could in principle be made more efficient using the same technique we describe here. Because the CVA allows the integral in Eq. (2) to be written as a sum of fixed-kernel convolutions, it can be computed without a nested integral, at the cost of performing a few FFTs. This approach scales as $O(\frac{V_{cell}}{\Delta V}\log\frac{V_{cell}}{\Delta V})$, as do

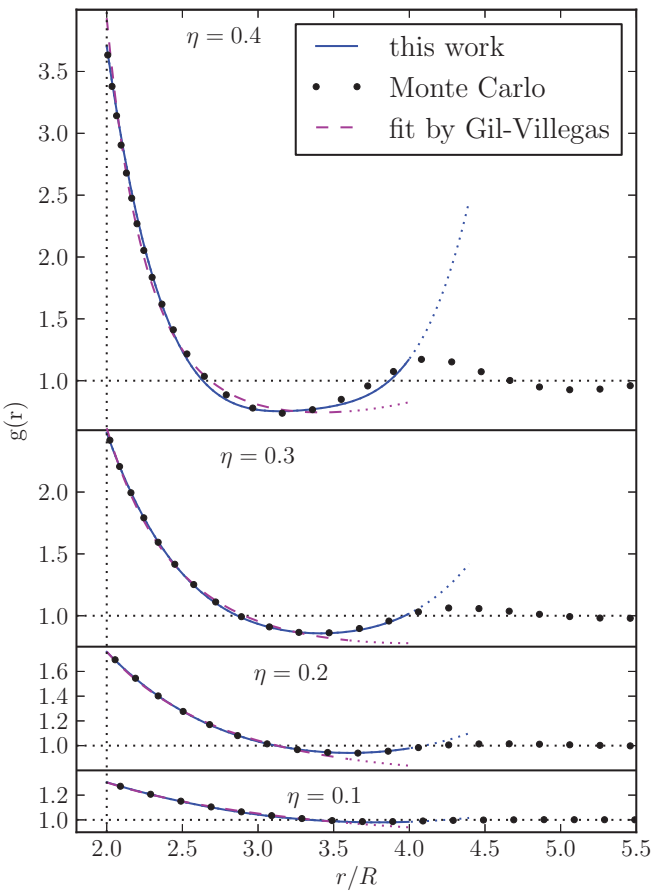

FIG. 1. (Color online) Plot of the hard-sphere radial distribution function of the homogeneous fluid at several values for packing fraction η. The blue lines show our separable fit, the black dots show the true radial distribution function $g(r)$ as found from Monte Carlo simulation, and the dashed lines are results of the Gil-Villegas fit [36]. The dotted extension of each fitted curve indicates the value of the function outside of the fitted region.

TABLE I. The fitted κ_{ij} matrix.

$$\kappa = \begin{pmatrix} -1.754 & 0.027 & 0.838 & -0.178 \\ -2.243 & 4.403 & -2.48 & 0.363 \\ 0.207 & 0.712 & -1.952 & 1.046 \\ -0.002 & -0.164 & 0.324 & -0.162 \end{pmatrix}$$

most widely used DFT functionals such as FMT [28,35]. With this scaling, when examining systems with long interaction distances or high resolution, which is often necessary when working with hard-sphere functionals, the CVA has the potential to be far more efficient than existing methods.

To see how we obtain this improved scaling, we examine the lowest-order correction in TPT, given by Eq. (2). The two terms that are averaged in Eq. (13) give equal contributions to the integral

$$F_1^{CVA} = \frac{1}{2}\iint g(r_{12}; g_\sigma(\mathbf{r}_2)) n(\mathbf{r}_1) n(\mathbf{r}_2) \Phi(|\mathbf{r}_1 - \mathbf{r}_2|)\, d\mathbf{r}_1\, d\mathbf{r}_2. \tag{16}$$

When we introduce the separable form for $g(r_{12}; g_\sigma)$ we can further simplify this integral as

$$F_1^{CVA} = \sum_i \frac{1}{2}\int n(\mathbf{r}_1) \int a_i(r_{12}) \Phi(r_{12}) b_i[g_\sigma(\mathbf{r}_2)] n(\mathbf{r}_2)\, d\mathbf{r}_2\, d\mathbf{r}_1, \tag{17}$$

where the functional is written as a summation of integrals of simple convolutions in three dimensions. Thus, each of these integrals may be computed in $O(N \log N)$ time, where N is the number of grid points in the computational cell. This is the same scaling as is required to compute the fundamental measures such as n_3 which are used in FMT.

VI. A SEPARABLE FIT FOR THE RADIAL DISTRIBUTION FUNCTION

Having settled on the basic structure of our function, we further refine it by performing a separable fit to the radial distribution function from Monte Carlo simulation. We focus our fit on the range of distances $r_{12} \leqslant 4R$. This range is relevant to the widely used [37–39] Statistical Associating Fluid Theory of Variable Range (SAFT-VR) free energy with

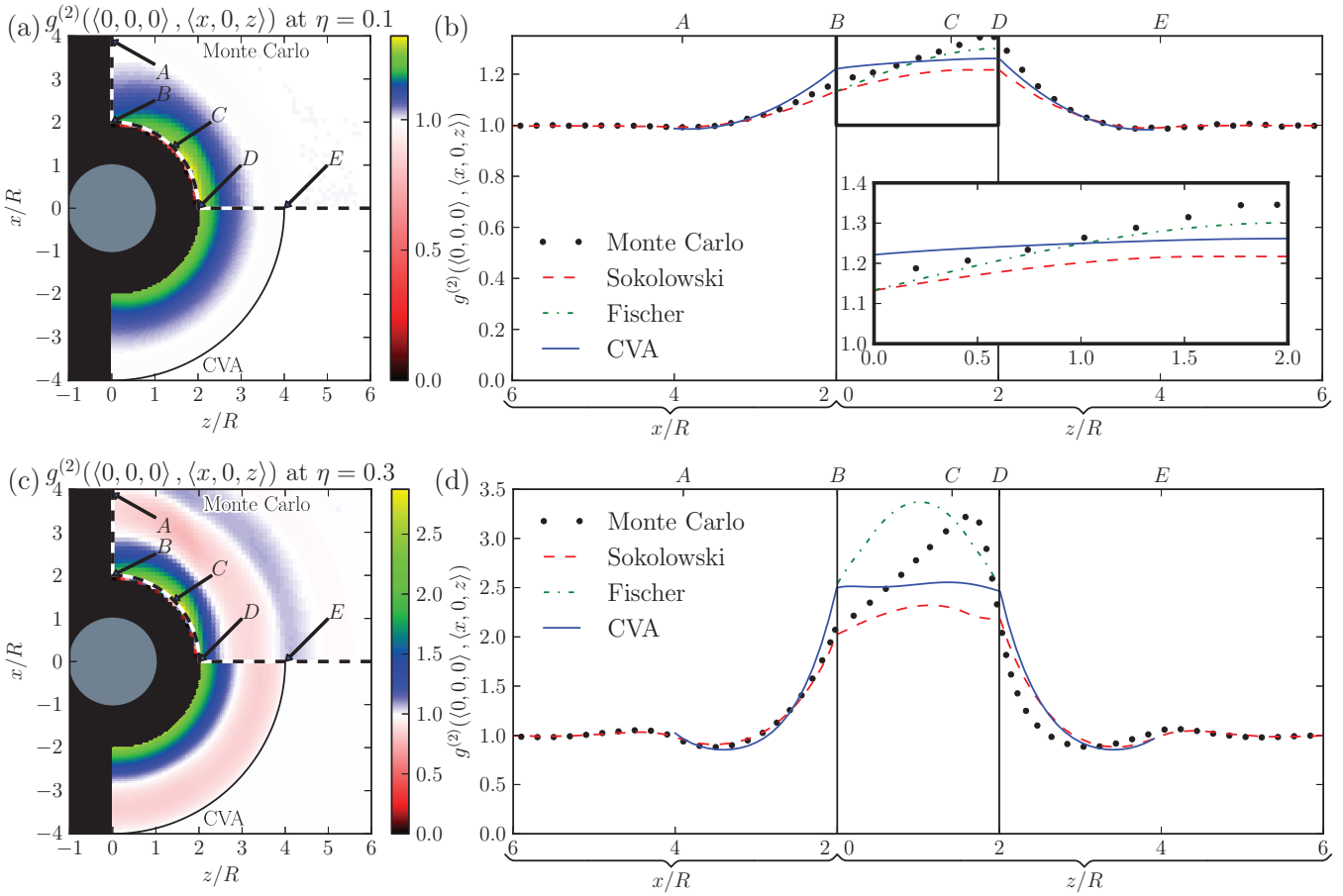

FIG. 2. (Color online) The pair distribution function near a hard wall, with packing fractions of 0.1 and 0.3 and $\mathbf{r}_1$ in contact with the hard wall. On the left are two-dimensional (2D) plots of $g^{(2)}(\mathbf{r}_1,\mathbf{r}_2)$ as $\mathbf{r}_2$ varies. The top halves of these figures show the results of Monte Carlo simulations, while the bottom halves show the CVA, truncated beyond the range of the fit. On the right are plots of $g^{(2)}(\mathbf{r}_1,\mathbf{r}_2)$ on the paths illustrated in the figures to the left. These plots compare the CVA (blue solid line), Monte Carlo results (black circles), the results of Sokolowski and Fischer (red dashed line) [31], and those of Fischer and Methfessel (green dot-dashed line) [26]. The latter is plotted only at contact, where it is defined.

square-well dispersive attraction developed by Gil-Villegas *et al.* [36]. Although we consider this range of radii particularly interesting, this is not a fundamental limit of the approach, as one could readily extend the fit to larger radii by including additional fitting parameters. For comparison, in Fig. 1 we plot our fit, Monte Carlo data, and the radial distribution function of Gil-Villegas *et al.*, which we have extracted from their approximation for the first term in the dispersion free energy given by Eq. (2).

For ease of implementation and future extension to larger radii, we fit the radial distribution function using a fourth-order polynomial. We constrain our functional form such that $g(r;g_\sigma)$ reduces to g_σ at contact and approaches $g(r)=1$ in the low-density limit. Incorporating these constraints we have the functional form

$$g(r;g_\sigma) = g_\sigma + \sum_{i=1}^{4}\sum_{j=1}^{4} \kappa_{ij}(g_\sigma - 1)^i \left(\frac{r}{\sigma} - 1\right)^j, \qquad (18)$$

where the matrix κ_{ij} is determined from a least-squares fit to Monte Carlo data for the radial distribution function, over the range $2R \leqslant r \leqslant 4R$, and for packing fractions $\eta \leqslant 0.45$. The resulting parameters are displayed in Table I. The maximum error in $g(r)$ within this range is 0.2, which occurs at $\eta = 0.45$ and $r = 3.7R$. Figure 1 displays our approximation at just under half of the densities that were included in the fit.

VII. RESULTS

A. Pair distribution function

We begin by examining the pair distribution function near a hard wall, with a focus on the case where one of the two spheres is in contact with the hard wall. Figures 2(a) and 2(c) compare the results of the CVA with Monte Carlo simulations at packing fractions of 0.1 and 0.3, respectively. We see reasonable agreement at the lower density, with a flatter angular dependence when the two spheres are in contact. At the higher density, we see significant structure developing in the simulation results that is not reflected in our approximation.

Figures 2(b) and 2(d) show the pair distribution function as plotted along paths illustrated in Figs. 2(a) and 2(c). These plots compare the CVA with Monte Carlo results, as well as the approximations of Sokolowski and Fischer [31] and of Fischer and Methfessel [26] at the same packing fractions of 0.1 and 0.3. The approach of Fischer and Methfessel is defined only when the two spheres are in contact and is therefore only

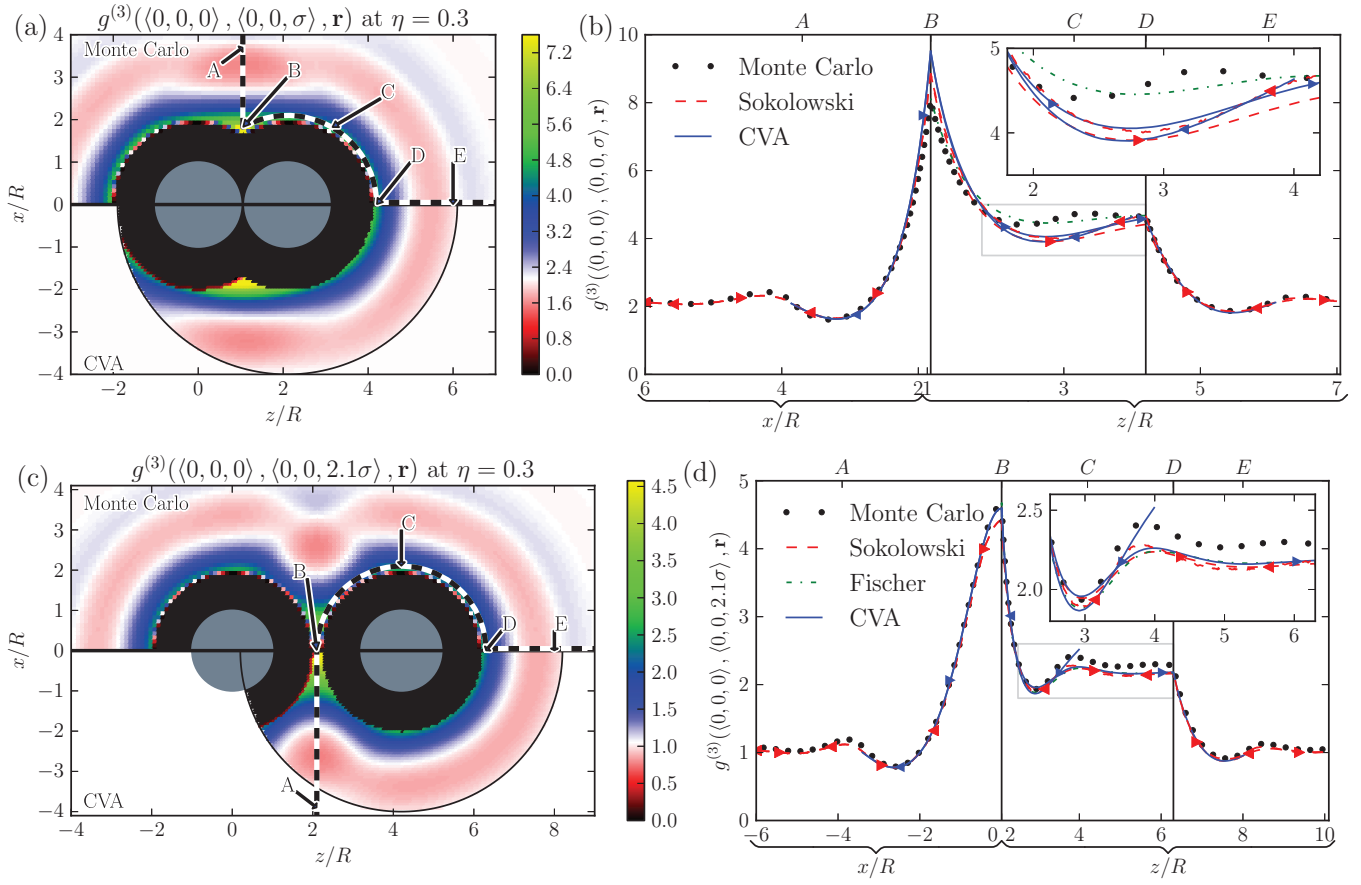

FIG. 3. (Color online) The triplet distribution function $g^{(3)}(\mathbf{r}_1,\mathbf{r}_2,\mathbf{r}_3)$ at packing fraction 0.3, plotted when $\mathbf{r}_1$ and $\mathbf{r}_2$ are in contact (a, b) and when $\mathbf{r}_1$ and $\mathbf{r}_2$ are separated by a distance 2.1σ (c, d). On the left are 2D plots of $g^{(3)}(\mathbf{r}_1,\mathbf{r}_2,\mathbf{r}_3)$ as $\mathbf{r}_3$ varies. The top halves of these figures show the results of Monte Carlo simulations, while the bottom halves show the CVA, truncated beyond the range of the fit. On the right are plots of $g^{(3)}(\mathbf{r}_1,\mathbf{r}_2,\mathbf{r}_3)$ on the paths illustrated in the figures to the left. We also plot these curves along a left-right mirror image of this path. The data for the right-hand paths (as shown in the 2D images) are marked with right-pointing triangles, while the left-hand paths are marked with left-pointing triangles.

plotted on that segment of the path. As an input to the previous approximations we use the hard sphere radial distribution function found with Monte Carlo simulation, interpolated as necessary. We find that both previous approximations to the pair distribution function predict stronger angular dependence of the pair distribution function at contact than this work. The previous approximations each have a systematic error at contact, either too high or too low. In contrast, our errors at contact have a tendency to cancel when used in a perturbation expansion. At higher densities, the approximation of Fischer and Methfessel requires evaluating the radial distribution function at densities significantly higher than the freezing density, which poses numerical difficulties when using the radial distribution function from simulation. When the two points $\mathbf{r}_1$ and $\mathbf{r}_2$ are both more than a radius away from contact, we find that any of these approaches gives a reasonable prediction.

B. Triplet distribution function

Just as the radial distribution function of a homogeneous fluid may be computed from the density of an inhomogeneous one using Percus's test-particle trick, the triplet distribution function of a homogeneous system can be computed using an approximation of the pair distribution for an inhomogeneous fluid, such as we have developed. The triplet distribution function of a homogeneous fluid with density n is given by

$$g^{(3)}(\mathbf{r}_1,\mathbf{r}_2,\mathbf{r}_3) = \frac{n_{\mathrm{TP}(\mathbf{r}_1)}(\mathbf{r}_2) n_{\mathrm{TP}(\mathbf{r}_1)}(\mathbf{r}_3)}{n^2} g^{(2)}_{\mathrm{TP}(\mathbf{r}_1)}(\mathbf{r}_2,\mathbf{r}_3), \tag{19}$$

where the $\mathrm{TP}(\mathbf{r}_1)$ subscript indicates quantities computed for the inhomogeneous density configuration in which one sphere (the "test particle") is fixed at position $\mathbf{r}_1$. This method treats one of the three positions, the location of the test particle, differently from the other two, which means that a poor approximation to the pair distribution function may break the symmetry between $\mathbf{r}_1$ and $\mathbf{r}_2$ which is present in the true triplet distribution function.

Figures 3(a) and 3(c) compare the triplet distribution function at a packing fraction of 0.3 computed using the CVA with results from Monte Carlo simulations. In Fig. 3(a) the spheres at $\mathbf{r}_1$ and $\mathbf{r}_2$ are in contact; in Fig. 3(c) they are spaced so that a third sphere can just fit between them; and in both figures $\mathbf{r}_3$ is varied. The test-particle position for the CVA in each case is $\mathbf{r}_1$, which is on the left-hand side of the figure. As before, we see reasonable agreement with simulation. Also, the Monte Carlo results have the expected left-right symmetry, while the CVA has a small asymmetry introduced with the test particle due to errors in the pair distribution function.

Figures 3(b) and 3(d) show the triplet distribution function as plotted along the paths illustrated in Figs. 3(a) and 3(c). We also plot the results along a left-right mirror image path, corresponding to swapping $\mathbf{r}_1$ and $\mathbf{r}_2$. The two mirror-image paths are distinguished by arrows (triangles) along the curves, with right-facing arrows indicating the paths shown in Figs. 3(a) and 3(c), and left-facing arrows indicating the mirror image path. As the work of Fischer and Methfessel is only defined when $\mathbf{r}_2$ and $\mathbf{r}_3$ are in contact, we plot it only along the central portion of the path, which is in contact with $\mathbf{r}_2$, and arrows are omitted. All methods tested perform similarly over their range of validity.

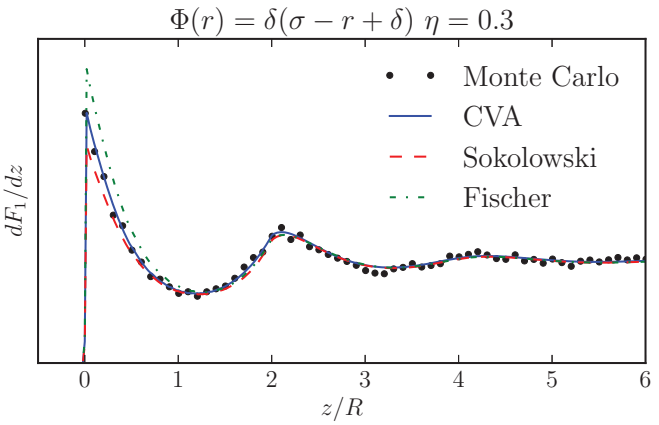

(a) Sticky hard-sphere fluid

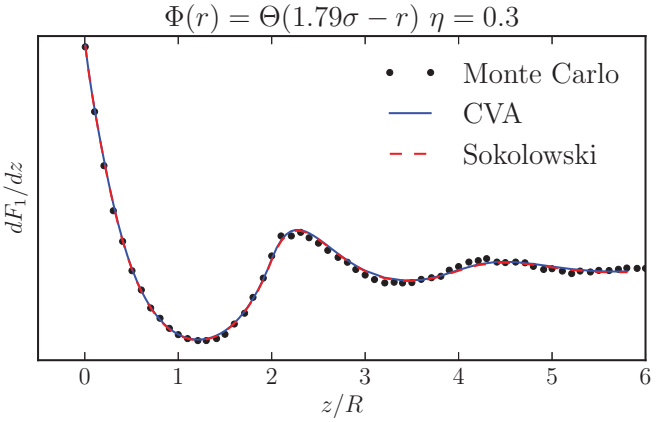

(b) Hard-core square well fluid

FIG. 4. (Color online) Plot of $\frac{dF_1}{dz}$ near a hard wall, with arbitrary vertical scale. (a) A sticky hard-sphere fluid defined by a pair potential $\delta(\sigma - r + \delta)$, where σ is the hard-sphere diameter and δ is an infinitesimal distance; (b) a square well fluid defined by a pair potential $\Theta(1.79\sigma - r)$.

VIII. ACCURACY IN THERMODYNAMIC PERTURBATION THEORY

A particularly relevant quantitative test of a pair distribution function is how well it predicts the interaction energy due to a pair potential. To this end, we have computed the error in the first term in a high-temperature perturbation expansion F_1 for two typical pair potentials. In order to focus on effects at the interface, we have defined a position-dependent pair interaction energy as

$$\frac{dF_1}{dz} = \frac{1}{2}\int g^{(2)}_{HS}(\mathbf{r},\mathbf{r}') n(\mathbf{r}) n(\mathbf{r}') \Phi(|\mathbf{r}-\mathbf{r}'|)\, d\mathbf{r}'\, dx\, dy, \tag{20}$$

which gives the contribution to the mean-field free energy due to molecules located in a plane of fixed z.

We plot this quantity for two representative pair potentials near a hard wall in Fig. 4. We have chosen to illustrate a δ function interaction at contact (i.e., "sticky hard spheres"), and a hard-core square-well fluid, with the length-scale of

interaction taken from the optimal SAFT model for water found by Clark *et al.* [8]. These pair potentials represent both a very short-range interaction and a medium-range interaction.

Figure 4(a) shows the results for the sticky hard-sphere fluid. The CVA is constructed to produce this result exactly, provided the averaged pair distribution function at contact from Ref. [34] is exact. As expected, we see excellent agreement with the Monte Carlo simulation results, while the approximations of Fischer and Sokolowski each show deviations near the interface. Figure 4(b) shows the same curve from Eq. (20) for the square-well fluid. In this case both the CVA and Sokolowski's approximation give excellent agreement with simulation.

IX. CONCLUSION

We have introduced and tested the contact value approach for the pair distribution function $g^{(2)}(\mathbf{r}_1,\mathbf{r}_2)$ of the inhomogeneous hard-sphere fluid. The pair distribution function plays a key role in thermodynamic perturbation theory, which is widely used in the construction of classical density functionals. The CVA, unlike existing approximations, is suitable for use in classical density functionals based on perturbation theory, as it may be efficiently computed using exclusively fixed-kernel convolutions. We have tested this function at a hard wall and near a single fixed hard sphere, and find that it gives excellent agreement with simulation. Tests of the pair distribution function in integrals that arise in thermodynamic perturbation theory suggest that the CVA is accurate for attractions up to the distance to which the radial distribution function is fit and is a significant improvement over existing approximations near contact. But most importantly, the computational cost of using the CVA in a classical density functional scales much more favorably than existing methods in high-resolution computations.

[1] J. Hansen and I. McDonald, *Theory of Simple Liquids* (Elsevier Science, London, 2006).
[2] S. Jain, A. Dominik, and W. G. Chapman, J. Chem. Phys. **127**, 244904 (2007).
[3] G. J. Gloor, G. Jackson, F. Blas, E. M. Del Rio, and E. De Miguel, J. Phys. Chem. C **111**, 15513 (2007).
[4] J. Gross, J. Chem. Phys. **131**, 204705 (2009).
[5] H. Kahl and J. Winkelmann, Fluid Phase Equilibria **270**, 50 (2008).
[6] J. Hughes, E. J. Krebs, and D. Roundy, J. Chem. Phys. **138**, 024509 (2013).
[7] P. Bryk, S. Sokołowski, and O. Pizio, J. Chem. Phys. **125**, 024909 (2006).
[8] G. Clark, A. Haslam, A. Galindo, and G. Jackson, Mol. Phys. **104**, 3561 (2006).
[9] R. Sundararaman, K. Letchworth-Weaver, and T. Arias, J. Chem. Phys. **137**, 044107 (2012).
[10] B. D. Marshall and W. G. Chapman, J. Chem. Phys. **138**, 044901 (2013).
[11] M. Plischke and D. Henderson, Proc. R. Soc. Lond. A **404**, 323 (1986).
[12] F. Lado, Mol. Phys. **107**, 301 (2009).
[13] A. González, F. Román, and J. White, J. Phys. Condens. Matter **11**, 3789 (1999).
[14] B. Götzelmann, A. Haase, and S. Dietrich, Phys. Rev. E **53**, 3456 (1996).
[15] R. Paul and S. J. Paddison, Phys. Rev. E **67**, 016108 (2003).
[16] S. Toxvaerd, Mol. Phys. **26**, 91 (1973).
[17] J. Pressing and J. E. Mayer, J. Chem. Phys. **59**, 2711 (1973).
[18] S. J. Salter and H. T. Davis, J. Chem. Phys. **63**, 3295 (1975).
[19] V. Bongiorno and H. T. Davis, Phys. Rev. A **12**, 2213 (1975).
[20] S. Toxvaerd, J. Chem. Phys. **64**, 2863 (1976).
[21] M. Kalos, J. Percus, and M. Rao, J. Stat. Phys. **17**, 111 (1977).
[22] B. S. Carey, L. E. Scriven, and H. T. Davis, J. Chem. Phys. **69**, 5040 (1978).
[23] T. R. Osborn and C. A. Croxton, Mol. Phys. **40**, 1489 (1980).
[24] B. McCoy, L. Scriven, and H. Davis, J. Chem. Phys. **75**, 4719 (1981).
[25] J. C. Barrett, J. Chem. Phys. **124**, 144705 (2006).
[26] J. Fischer and M. Methfessel, Phys. Rev. A **22**, 2836 (1980).
[27] J. Harris and S. A. Rice, J. Chem. Phys. **86**, 5731 (1987).
[28] Y. Rosenfeld, Phys. Rev. Lett. **63**, 980 (1989).
[29] Z. Tang, L. Scriven, and H. Davis, J. Chem. Phys. **95**, 2659 (1991).
[30] P. Tarazona, Phys. Rev. A **31**, 2672 (1985).
[31] S. Sokolowski and J. Fischer, J. Chem. Phys. **96**, 5441 (1992).
[32] T. Wadewitz and J. Winkelmann, J. Chem. Phys. **113**, 2447 (2000).
[33] J. Winkelmann, J. Phys. Condens. Matter **13**, 4739 (2001).
[34] J. B. Schulte, P. A. Kreitzberg, C. V. Haglund, and D. Roundy, Phys. Rev. E **86**, 061201 (2012).
[35] R. Roth, R. Evans, A. Lang, and G. Kahl, J. Phys. Condens. Matter **14**, 12063 (2002).
[36] A. Gil-Villegas, A. Galindo, P. J. Whitehead, S. J. Mills, G. Jackson, and A. N. Burgess, J. Chem. Phys. **106**, 4168 (1997).
[37] W. Chapman, K. Gubbins, G. Jackson, and M. Radosz, Fluid Phase Equilibria **52**, 31 (1989).
[38] E. A. Müller and K. E. Gubbins, Ind. Eng. Chem. Res. **40**, 2193 (2001).
[39] S. P. Tan, H. Adidharma, and M. Radosz, Ind. Eng. Chem. Res. **47**, 8063 (2008).